Electron Delocalization in Mixed-Valence Tungsten Polyanions

C. Sanchez,[1a] J. Livage,*[1a] J. P. Launay,[1b] and M. Fournier[1c]

Contribution from Spectrochimie du Solide, Chimie des Métaux de Transition and Physico-Chimie Inorganique, Université Pierre et Marie Curie, 75230 Paris, Cedex 05, France.
Received December 20, 1982

Abstract: Electron transfer in mixed-valence tungsten polyanions has been studied by ESR and optical spectroscopy. Several series of compounds belonging to the (W_6O_{19}), $(XW_{12}O_{40})$, $(As_2W_{18}O_{62})$, and $(AsH_2W_{18}O_{60})$ structural types have been considered. All these polyanions belong to class II according to the Robin and Day classification. The thermal activation energy was calculated from a detailed analysis of the ESR line width in the 4–200 K temperature range. Optical activation energies were deduced from the position of the intervalence transfer absorption bands. A comparison of both results gave an estimate of the transfer integral J between tungsten sites. The thermally activated electron hopping strongly depends on the junction between adjacent WO_6 octahedra. Delocalization appears to be easier between corner sharing octahedra. On the other hand, substitution of one tungsten by a foreign atom leads to a stronger localization of the unpaired electron.

In a previous paper,[2] we reported a study of electron delocalization in mixed-valence molybdenum polyanions. These were one-electron reduced Lindqvist $(Mo_6O_{19})^{3-}$ or Keggin polyanions $(XMo_{12}O_{40})^{n-}$ and $(SiMo_3W_9O_{40})^{5-}$. ESR experiments showed that, at low enough temperatures (below 40 K), the unpaired electron remains trapped on a single molybdenum site. A thermally activated electron hopping was observed at higher temperatures, leading to a broadening of the ESR spectra. It was possible, from computer simulation, to calculate the dependence of line width on temperature and therefore the hopping frequency of the unpaired electron. A thermal activation energy was thus estimated. The optical activation energy was deduced from the position of the so-called "intervalence transition". A comparison of both activation energies, using the equation[3]

$$E_{th} = {}^1/_4E_{op} - J + (J^2/E_{op}) \quad (1)$$

led to an estimate of the transfer integral J allowing a discussion of the amount of electronic interaction between molybdenum ions in both polyanions.

This electronic interaction appeared to be larger when MoO_6 octahedra were sharing corners rather than edges. Such a result is in agreement with other observations made by Pope[4] on $(SiW_9V_3O_{40})^{8-}$ and $(P_2W_{15}V_3O_{62})^{10-}$.

In this paper, we extend our study to tungsten polyanions. Four different structural types are investigated, namely, hexatungstates[5] $(W_6O_{19})^{2-}$, dodecatungstates $(XW_{12}O_{40})^{n-}$ (Keggin[6] structure), and two types of octadecatungstates, $(As_2{}^{V}W_{18}O_{60})^{6-}$[7] and $(As^{III}{}_2H_2W_{18}O_{62})^{7-}$.[8] Earlier ESR results, published by Prados and Pope[9] in 1976 on $(XW_{12}O_{40})^{n-}$ and $(X_2W_{18}O_{62})^{n-}$ polyanions, were interpreted by assuming that at low temperatures, the unpaired electron remains trapped on a single tungsten site in an orthorhombic ligand field, a result in agreement with the C_s symmetry of the basic WO_6 octahedron. No hyperfine structure with the ^{183}W isotope ($I = {}^1/_2$) was observed. Such hyperfine coupling is, however, reported here for the $(W_6O_{19})^{3-}$ polyanion, unambiguously showing the electron localization on a single tungsten site. The transfer integral J is deduced from ESR and optical measurements. As for molybdenum polyanions, J is lowest in the $(M_6O_{19})^{3-}$ structure. Finally, the electronic spectra of $(As_2W_{18}O_{62})^{7-}$ and $(AsH_2W_{18}O_{60})^{8-}$ have been reinvestigated. Low-energy intervalence transfer absorption has been found around 5000 cm^{-1}. Its attribution is discussed.

Experimental Section

Preparations. $(NBu_4)_2[W_6O_{19}]$. This polyanion was prepared according to the procedure previously described[10] for $(Mo_6O_{19})^{2-}$. A suspension of 33 g of $Na_2WO_4 2H_2O$ (10^{-1} mol) was stirred in an acetic anhydride (40 mL)–dimethylformamide (30 mL) mixture for 3 h at 100 °C until a fluid paste was obtained. A mixture of acetic anhydride (20 mL), dimethylformamide (50 mL), and concentrated hydrochloric acid (18 mL) was then added. After 2 h at 100 °C, the white residue was filtered and the solution precipitated by a NBu_4Br methanolic solution (15 g in 50 mL) and 28 g of crude product was filtered off. Recrystallization in Me_2SO yielded 21 g of colorless blocks: IR (cm^{-1}, an asterisk indicates a cation band) 975 (vs), 888* (vw), 882* (vw), 873* (vw), 812 (vs), 752* (vw), 736* (vw), 716* (vw), 664* (vw), 588 (s), 445 (vs), 402* (vw), 368 (vs).

$(NBu_4)_3[NbW_5O_{19}]$. The preparation previously described[11] was modified as follows: 11.2 g of $K_8Nb_6O_{19}\cdot 10H_2O$ (8×10^{-3} mol) was dissolved into 200 mL of water and 200 mL of 1 M Na_2WO_4 (0.2 mol) and 10 mL of 110 volume H_2O_2 (0.1 mol) were then added together with 60 mL of 6 N H_2SO_4 until pH 2.5 was reached. The resulting solution turned orange. It was then refluxed for 5 h until all peroxo compounds were decomposed (the solution turned yellowish). The hot solution was quickly filtered in order to eliminate the unreacted niobium polymer. A tetramethylammonium chloride aqueous solution (15 g in 100 mL) was added to the hot filtrate which yielded 35 g of crude product. Recrystallization was performed in 1400 mL of boiling water giving 18 g of pure refringent crystals. The purity of this salt was checked by polarography (DME, formiate buffer pH 3.6, $E_{1/2} = -0.85$ V vs. SCE). The NBu_4^+ salt was obtained from an aqueous NMe_4^+ salt solution by precipitation with $NBu_4^+Br^-$ and recrystallization in DMF. IR (cm^{-1}, an asterisk indicates a cation band) 958 (vs), 916 (s), 885* (w), 803 (vs), 736* (w), 682* (vw), 590 (m), 575 (m), 440 (vs), 433 (sh), 370 (vw), 349 (w).

α-$Na_6[H_2W_{12}O_{40}]\cdot nH_2O$. This preparation, using the dissolution of stoichiometric $Na_2WO_4\cdot 2H_2O$ in a $WO_3\cdot H_2O$ reactive suspension, was

(1) (a) Laboratoire de Spectrochimie du Solide, LA 302. (b) Laboratoire de Chimie des Métaux de Transition, ERA 608. (c) Laboratoire de Physicochimie inorganique, ERA 608.

(2) Sanchez, C.; Livage, J.; Launay, J. P.; Fournier, M.; Jeannin, Y. *J. Am. Chem. Soc.* **1982**, *104*, 3194.

(3) (a) Wong, K. Y.; Schatz, P. N.; Piepho, S. B. *J. Am. Chem. Soc.* **1979**, *101*, 2793. (b) Cannon, R. "Electron Transfer Reactions"; Butterworths: London, 1980; p 274.

(4) Mossoba, M. M.; O'Connor, C. J.; Pope, M. T.; Sinn, E.; Hervé, G.; Tézé, A. *J. Am. Chem. Soc.* **1980**, *102*, 6864. Harmalker, S. P.; Pope, M. T. *J. Am. Chem. Soc.* **1981**, *103*, 7381. Pope, M. T., private communication.

(5) The crystal structure of $[W_6O_{19}]^{2-}$ is described in the following papers: Henning, G.; Hüllen, A. *Z. Kristallogr.* **1969**, *130*, 162. Fuchs, J.; Freiwald, W.; Hartl, H. *Acta Crystallogr., Sect. B* **1978**, *34B*, 1764. La Rue, W. A.; Thu Liu, A.; San Filippo, J. *Inorg. Chem.* **1980**, *19*, 315. Kirillova, N. I.; Kolomonikov I. S.; Zolotarev, Y. A.; Lysyok, T. V.; Struchkov, Y. T. *Koord. Khim.* **1977**, *3*, 1895.

(6) The crystal structure of α-$[SiW_{12}O_{40}]^{4-}$ is described in the following: Kobayashi, A.; Sasaki, Y. *Bull. Chem. Soc. Jpn.* **1975**, *48*, 885. Smith, P. Ph.D. Thesis, Georgetown University, 1971; *Diss. Abstr. Int. B* **1972**, *32*, 5136. Fuchs, J.; Thiele, A.; Palm, R. *Z. Naturforsch.* **1981**, *36B*, 161. No structural determination seems to have been performed on the true metatungstate anion α-$[H_2W_{12}O_{40}]^{6-}$. The structure of a protonated form is described in the following: Fuchs, J.; Flindt, E. P. *Z. Naturforsch.* **1979**, *34B*, 412. The structure of the 6-electron reduced form has also been investigated: Jeannin, Y.; Launay, J. P.; Seid Sedjadi, M. A. *Inorg. Chem.* **1980**, *19*, 2933.

(7) Dawson, B. *Acta Crystallogr.* **1953**, *6*, 113; D'Amour, H. *Acta Crystallogr., Sect. B* **1976**, *B32*, 729.

(8) Jeannin, Y.; Martin-Frère, J. *Inorg. Chem.* **1979**, *18*, 3010.

(9) Prados, R. A.; Pope, M. T. *Inorg. Chem.* **1976**, *15*, 2547.

(10) Che, M.; Fournier, M.; Launay, J. P. *J. Chem. Phys.* **1979**, *71*, 1954.

(11) Dabbabi, M.; Boyer, M. *J. Inorg. Nucl. Chem.* **1976**, *38*, 1011.

0002-7863/83/1505-6817$01.50/0

Table I. Conditions for Electrochemical Reductions

product	concn	solvent	supporting electrolyte	imposed potential (vs SCE)
$(NBu_4)_2[W_6O_{19}]$	5×10^{-2}	Me_2SO or DMF	0.2 M $NBu_4^+BF_4^-$	−1.15
$(NBu_4)_3[NbW_5O_{19}]$	7×10^{-3}	DMF	0.2 M $NBu_4^+BF_4^-$	−2.2
α-$H_4[SiW_{12}O_{40}]$	1×10^{-2}	H_2O	0.5 M HCl	−0.4
α-$Na_6[H_2W_{12}O_{40}]$	1×10^{-2}	H_2O	1 M NaCl + phosphate buffer, pH 7	−0.7
α-$(NH_4)_6[As_2W_{18}O_{62}]$	1×10^{-2}	H_2O	0.1 M HCl	−0.3
$(NH_4)_7[AsH_2W_{18}O_{60}]$	5×10^{-3}	H_2O	1 M NaCl + acetate buffer, pH 3.5	−0.3

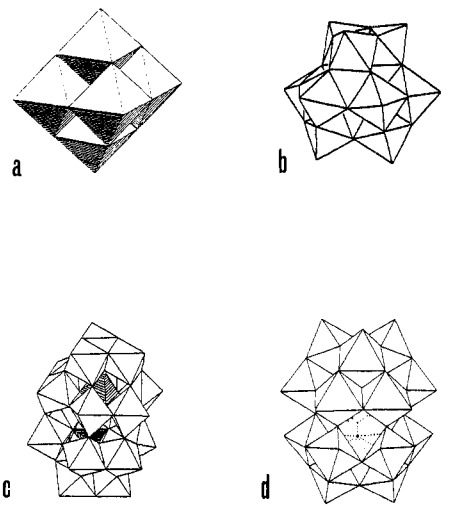

Figure 1. Structures of polytungstates: (a) anion $(W_6O_{19})^{2-}$; (b) anion $(SiW_{12}O_{40})^{4-}$; (c) anion $(As_2W_{18}O_{62})^{6-}$; and (d) anion $(AsH_2W_{18}O_{60})^{7-}$.

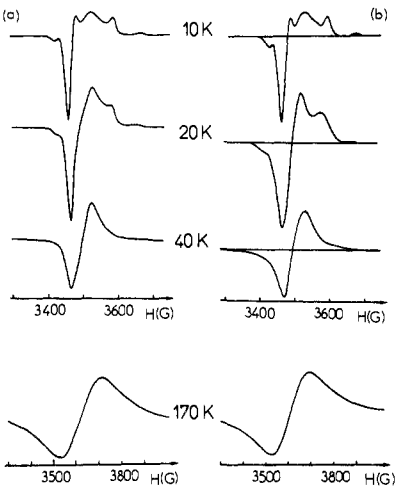

Figure 2. ESR spectra of $(W_6O_{19})^{3-}$: (a) experimental; (b) simulated.

described by Copaux.[12] Additional details on the preparation of $WO_3 \cdot H_2O$ can be found in ref 2 describing the preparation of $MoW_5O_{19}^{2-}$. The resulting solution was then refluxed for 5 h until the baryum test remained negative (no precipitation should be observed upon addition of a $BaCl_2$ solution). After filtration, an equal volume of DMF was added and the water slowly evaporated. Small crystals were obtained, which could be recrystallized in water. The purity was checked by polarography ($E_{1/2}$ at pH 4 −0.62 (2 F), −0.82 (2 F), −1.00 (12 F) V vs. SCE).

α-$H_4[SiW_{12}O_{40}] \cdot 19H_2O$ was prepared by Copaux's method,[13] followed by ether extraction. Polarography: $E_{1/2}$ vs. SCE in a sodium acetate (1 M)/acetic acid (1 M) mixture, −0.26 (1 F), −0.52 (1 F), −0.95 (2 F) V.

α-$(NH_4)_6[As_2W_{18}O_{62}] \cdot nH_2O$ was prepared by Kehrmann's method.[14] Polarography was performed on a rotating glassy carbon electrode in a $HClO_4$ (0.1 M) − $NaClO_4$ (0.9 M) mixture: +0.086 (1 F), −0.087 (1 F), −0.400 (2 F), −0.640 (2 F) V vs. SCE.

$(NH_4)_7[H_2AsW_{18}O_{60}] \cdot 16H_2O$ was kindly supplied by J. Martin-Frère.[8]

Electrochemical Reductions. These were performed on a mercury cathode according to the conditions given in Table I. The solutions containing $[W_6O_{19}]^{3-}$ and $[NbW_5O_{19}]^{4-}$ were found to be *extremely air-sensitive*. They were transfered in argon-flushed ESR tubes using an argon inflated glove bag. In order to prevent crystallization upon cooling during ESR experiments, the aqueous solutions were mixed with 10% ethylene glycol.

Spectroscopy. Electronic spectra were recorded with a Beckman 5240 UV–visible spectrophotometer between 2000 and 400 nm. X-band ESR spectra were recorded on a JEOL ME 3X spectrometer. Low-temperature experiments down to 4 K were performed with an Oxford Instrument cryostat. The magnetic field was measured with an NMR proton probe and the microwave frequency with a wavemeter giving an accuracy of ±1 MHz.

Results

Electron Spin Resonance. $[W_6O_{19}]^{3-}$. The ESR spectra in Me_2SO are given in Figure 2a. The frozen solution spectrum recorded at 10 K exhibits both parallel and perpendicular features typical of a W(V) ion in an axial ligand field. The strong central line is due to the 86.74% abundant ^{182}W, ^{184}W, and ^{186}W isotopes ($I = 0$), while the weak lines arise from the hyperfine coupling with the ^{183}W isotope ($I = {}^1/_2$). The ESR spectrum can then be described by the following spin Hamiltonian:

$$\mathcal{H} = g_{//}\beta H_z S_z + g_\perp \beta (H_x S_x + H_y S_y) + A_{//} S_z I_z + A_\perp (S_x I_x + S_y I_y)$$

The main axis of both $\bar{g}$ and $\bar{A}$ tensors is taken along the distorsion axis z, i.e., along the W=O bond. When the natural isotopic abundance (^{183}W = 14%) is taken into account, the magnetic parameters can be deduced from a computer simulation using a Gaussian line shape (Figure 2b). The results are reported in Table

Table II. Electron Spin Resonance Parameters of Reduced Polytungstates

polyanions	g_x	g_y	g_z	ΔH_{pp} (G) (T = 10 K) Δx	Δy	Δz	ref
							$A_\parallel$ = 158 G
$(W_6O_{19})^{3-}$	1.76	1.76	1.703	20	20	20	$A_\perp$ = 74 G[a]
$(W_5NbO_{19})^{4-}$	1.742	1.722	1.684	64	64	72	a
$(SiW_{12}O_{40})^{5-}$	1.854	1.826	1.784	30	32	40	a
$(H_2W_{12}O_{40})^{7-}$	1.854	1.803	1.755	40	45	44	a
$(HF_3W_{12}O_{37})^{5-}$	1.853	1.821	1.778	30	30	40	(28)
$(GeW_{12}O_{40})^{5-}$	1.848	1.816	1.779				(9)
$(BW_{12}O_{40})^{6-}$	1.854	1.823	1.773				(9)
$(As_2W_{18}O_{62})^{7-}$	1.812	1.849	1.907	30	30	20	a
$(H_2W_{18}F_6O_{56})^{9-}$	1.811	1.852	1.917	38	35	30	(28)
$(P_2W_{18}O_{62})^{7-}$	1.814	1.854	1.906				(9)
$(AsH_2W_{18}O_{60})^{8-}$	1.743	1.775	1.809[b]	34	30	20	a
	1.809	1.775	1.743				

[a] This work. [b] The two possibilities $g_z > g_x, g_y$ and $g_z < g_x$, g_y cannot be distinguished safely in this case.

(12) Copaux, H. *Ann. Chim. (Paris)* **1909**, *17*, 217.
(13) *Inorg. Synth.* **1939**, *1*, 129.
(14) Kehrmann, F. *Z. Anorg. Allg. Chem.* **1899**, *22*, 285.

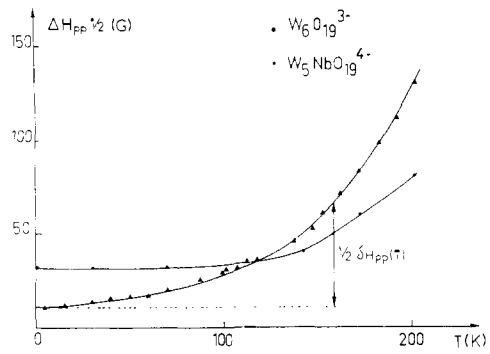

Figure 3. Temperature dependence of the ESR line width of $(W_6O_{19})^{3-}$ (▲) and $(W_5NbO_{19})^{4-}$ (●) ($^1/_2\Delta H_{pp}$ correspond to the peak-to-peak half-width).

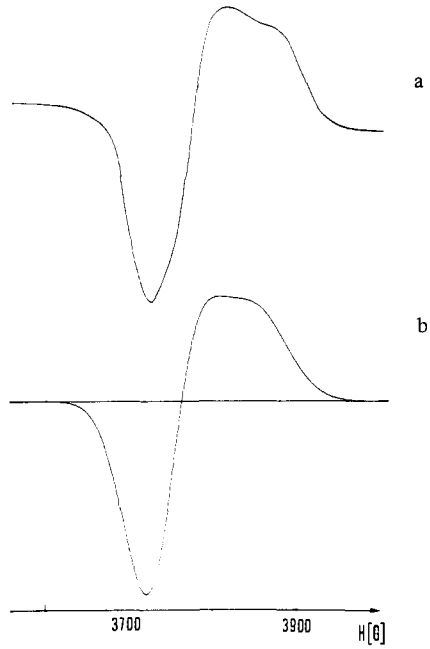

Figure 4. ESR spectrum of the one-electron reduced $(W_5NbO_{19})^{4-}$ polyanion recorded at 4 K: (a) experimental; (b) simulated.

II. It may be noticed that whatever the preparation could be, the spectrum of some tungsten impurity (about 5%) is observed around $g = 1.73$.

The temperature dependence of the ESR spectrum is also shown in figure 2, together with the corresponding computer simulation. A line broadening is observed when the temperature increases. The hyperfine components disappear around 25 K while the spectrum remains anisotropic. It then appears fully isotropic above 40 K and a continuous broadening is observed up to 200 K. Above this temperature, the solution is no longer frozen and molecular tumbling is observed. A computer simulation was performed (Figure 2b), using a Gaussian line shape below 40 K and a Lorentzian one above this temperature. A plot of the peak-to-peak half-width $^1/_2\Delta H_{pp}$ vs. temperature is reported in Figure 3.

$[NbW_5O_{19}]^{4-}$. The ESR spectrum of a solution in DMF is shown in Figure 4a. At 4 K, the frozen solution spectrum does not exhibit any hyperfine structure. This is probably due to a larger line width ($\Delta H_{pp} \sim 60$ G) than is usually observed in other polytungstates (about 30 G). The spectrum is typical of a W(V) ion in an orthorhombic ligand field and can be described by the following Zeeman Hamiltonian:

$$\mathcal{H} = g_x\beta H_x S_x + g_y\beta H_y S_y + g_z\beta H_z S_z$$

where z is taken along the W=O bond as previously. The ESR parameters, deduced from a computer simulation (Figure 4b), are reported in Table II.

A line broadening is observed above 77 K. The two low-field components begin to collapse first, suggesting that g_x and g_y are larger than g_z. A plot of the peak-to-peak half-width $^1/_2\Delta H_{pp}$ is shown in Figure 3.

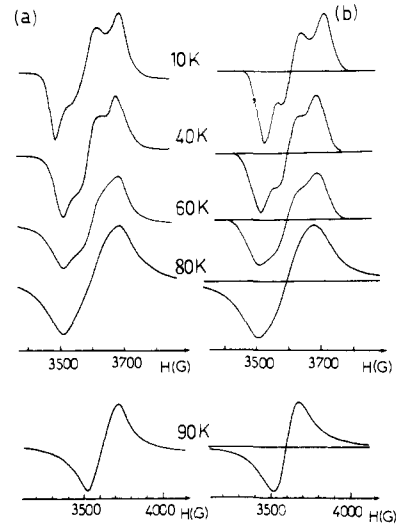

Figure 5. ESR spectra of $(H_2W_{12}O_{40})^{7-}$: (a) experimental; (b) simulated.

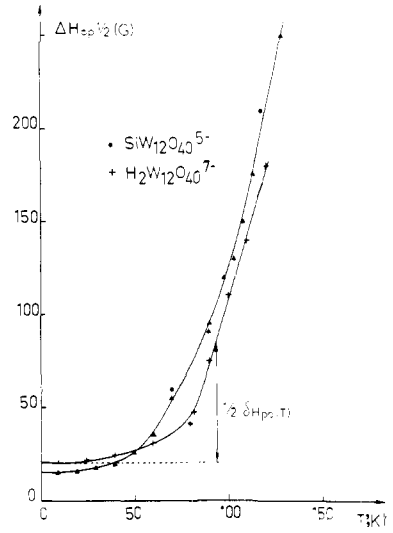

Figure 6. Temperature dependence of the ESR line width of $(H_2W_{12}O_{40})^{7-}$ (+) and $(SiW_{12}O_{40})^{5-}$ (▲) ($^1/_2\Delta H_{pp}$ correspond to the peak-to-peak half-width).

$[H_2W_{12}O_{40}]^{7-}$. The ESR spectrum of a $H_2W_{12}O_{40}^{7-}$ solution in water is shown in Figure 5a. No hyperfine structure is observed as previously reported by Pope.[9] The frozen solution spectrum, recorded at 10 K, is typical of a W(V) ion in an orthorhombic ligand field and can be described by a Zeeman spin Hamiltonian only. The magnetic parameters deduced from a computer simulation (Figure 5b) are reported in Table II.

A line broadening is observed above 35 K, and the ESR spectrum first appears to be axial around 75 K before being wholly isotropic above 85 K. As previously the two low-field components collapse first, suggesting that g_x and g_y are larger than g_z. The spectrum becomes too broad to be seen anymore above 125 K. The computer simulation (Figure 5b) was performed without modifying the g tensor and by using a Gaussian line shape below 80 K and a Lorentzian one above 85 K. Between these temperatures, both shapes had to be taken into account. The peak-to-peak half-width $^1/_2\Delta H_{pp}$ temperature dependence is reported in Figure 6.

$[SiW_{12}O_{40}]^{5-}$. The ESR spectrum of this compound is quite similar to the ESR spectrum of $[H_2W_{12}O_{40}]^{7-}$, and the corresponding results are reported in Table II and Figure 6.

$[As_2W_{18}O_{62}]^{7-}$. The ESR spectrum of a frozen solution in water appears to be orthorhombic at 10 K (Figure 7a). No hyperfine structure is observed, and the spectrum can be described with the

Table III. Spectral Data for Reduced Polytungstates in the UV-Visible and Near-Infrared Region

compound	band positions[a] (cm^{-1})			
$W_6O_{19}^{3-}$	24 300 (232)	19 000 (sh)	10 000 (310), 8 900 (sh), 7 700 (sh), 6 300 (sh)	
$NbW_5O_{19}^{4-}$	24 700 (313)		10 600 (386)	
$H_2W_{12}O_{40}^{7-}$	21 000 (sh)	14 500 (2100)	8 300 (1450)	
$SiW_{12}O_{40}^{5-}$	19 600 (1000)	13 700 (1850)	7 800 (1400)	
$As_2W_{18}O_{62}^{7-}$	17 200 (sh)	14 100 (3120)	11 000 (3770)	5 900 (1500)
$AsH_2W_{18}O_{60}^{8-}$	21 000 (sh) 16 400 (sh)	12 000 (3850)	9 450 (4400)	5 500 (1900)

[a] Molar extinction coefficients in parentheses; sh = shoulder.

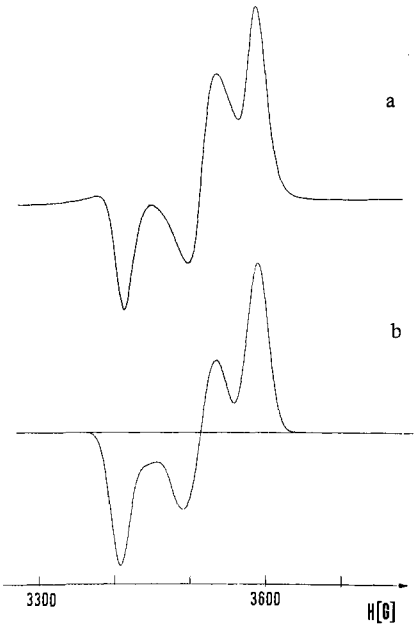

Figure 7. ESR spectrum of the one-electron reduced $(As_2W_{18}O_{62})^{7-}$ polyanion recorded at 10 K: (a) experimental; (b) simulated.

Zeeman spin Hamiltonian previously used. The corresponding ESR parameters deduced from a computer simulation are reported in Table II.

A line broadening is observed when the temperature increases, and the spectrum appears to be axial around 100 K and isotropic above 115 K. Contrary to the previous case, the two high-field components collapse first, indicating that g_x and g_y are now smaller than g_z. Such a behavior already has been reported by Pope.[9] The computer simulation was performed in the same way as for other polytungstates (Figure 7b), and the peak-to-peak half-width $^1/_2\Delta H_{pp}$ variation with temperature is shown in Figure 8.

$[AsH_2W_{18}O_{60}]^{8-}$. The ESR spectrum of a frozen solution in water is shown in Figure 9a. As previously, the spectrum recorded at 10 K is typical of a W(V) ion in an orthorhombic ligand field, and the ESR parameters deduced from a computer simulation are reported in Table II.

The temperature dependence of the ESR spectrum is also shown in Figure 9. A line broadening is observed, leading first to the collapse of the two high-field components. No purely axial spectrum is observed, however, and the spectrum becomes fully isotropic above 110 K. A computer simulation (Figure 9b) yielded the temperature dependence of the peak-to-peak half-width (Figure 8).

Electronic Spectra. Band positions and intensities are reported in Table III. The spectra of $[As_2W_{18}O_{62}]^{7-}$ and $[AsH_2W_{18}O_{60}]^{8-}$ are shown in Figure 10. The spectra of $[W_6O_{19}]^{3-}$ and $[NbW_5O_{19}]^{4-}$ are in general agreement with those already reported.[15] However, several shoulders were observed below 10 000 cm^{-1} in the case of $[W_6O_{19}]^{3-}$. The two species $[As_2W_{18}O_{62}]^{7-}$ and $[AsH_2W_{18}O_{60}]^{8-}$ exhibit bands at a surprisingly low energy (5900 and 5500 cm^{-1}, respectively); such bands have never been reported in previous works.

(15) Dabbabi, M.; Boyer, M.; Launay, J. P.; Jeannin, Y. *J. Electroanal. Chem.* **1977**, *76*, 153.

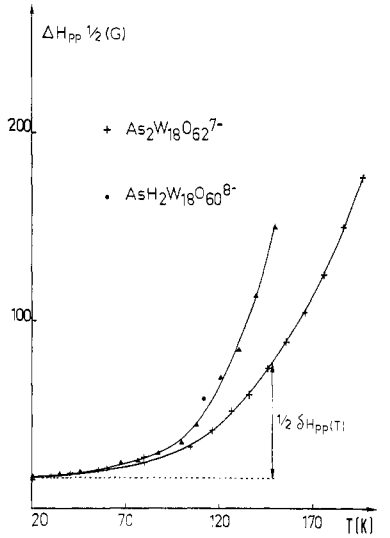

Figure 8. Temperature dependence of the ESR line width of $(As_2W_{18}O_{62})^{7-}$ (+) and $(AsH_2W_{18}O_{60})^{8-}$ (▲) ($^1/_2\Delta H_{pp}$ correspond to the peak-to-peak half-width).

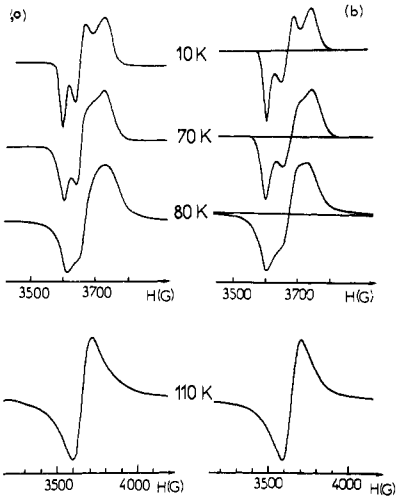

Figure 9. Temperature dependence of the ESR spectra of $(AsH_2W_{18}O_{60})^{8-}$: (a) experimental; (b) simulated.

Discussion

Valence Trapping and Ground-State Delocalization. ESR experiments show that, at very low temperatures, the unpaired electron remains localized on a single tungsten atom. The ESR spectrum appears to be orthorhombic, in good agreement with the local symmetry determined by X-ray diffraction experiments on non-reduced polyanions.[5-8] An axial spectrum, however, is observed for the $[W_6O_{19}]^{3-}$ anion. This result also agrees with structural data showing that the $(W_6O_{19})^{3-}$ structure is more symmetric than the others.

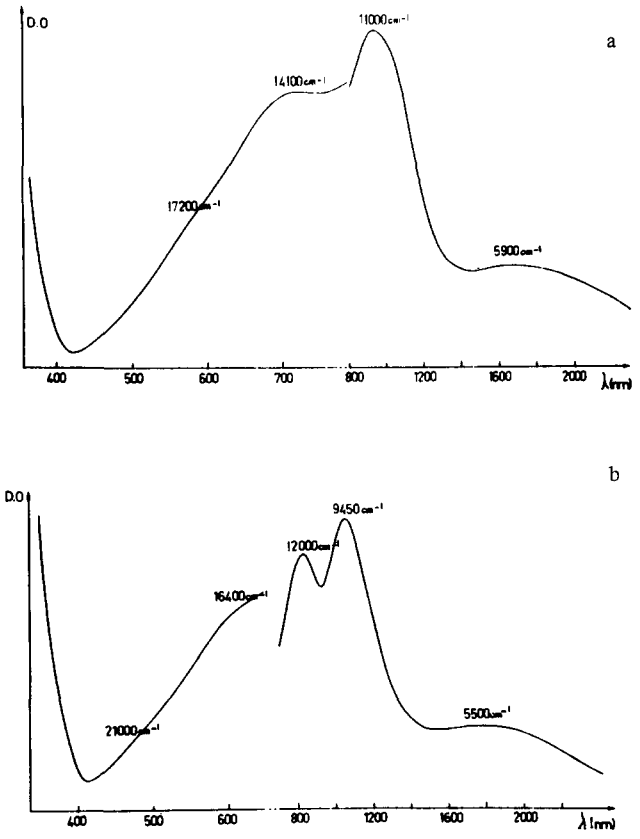

Figure 10. Electronic spectra of the one-electron reduced polyanions: (a) $(As_2W_{18}O_{62})^{7-}$; (b) $(AsH_2W_{18}O_{60})^{8-}$.

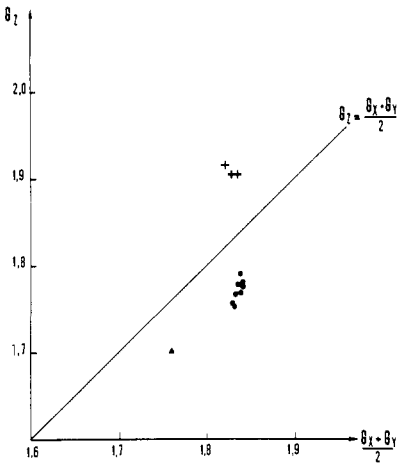

Figure 11. Diagram g_z vs. $^1/_2(g_x + g_y)$ for one-electron reduced polytungstates: (▲) $(W_6O_{19})^{3-}$; (●) $(XW_{12}O_{40})^{n-}$; (+) 2/18 structures.

The best evidence for electron localization, however, is provided by the well-resolved hyperfine structure of the $[W_6O_{19}]^{3-}$ ESR spectrum. Such a hyperfine coupling with the 14% abundant ^{183}W isotope has already been reported in monomeric tungsten ions.[16] But, to our knowledge this is the first case where it is observed in tungstate polyanions.[9] This presumably arises from a stronger electron localization in the ground state. The ESR line width also appears to be much smaller ($\Delta H \sim 18$ G) than for most other polyanions ($\Delta H \sim 30$ G).

g values for tungsten polyanions are somewhat larger than those for monomeric tungsten complexes.[16] This could be attributed to a larger degree of covalency in the ground state leading to a decrease of the spin–orbit coupling constant λ. A plot of $g_{//}$ vs. $^1/_2(g_x + g_y)$ (Figure 11) shows that this effect becomes more important when going from hexatungstate to dodecatungstate and octadecatungstate structures, i.e., when the condensation degree of the polyanion increases.

Table IV. Thermal Activation Energies, Optical Activation Energies, and Transfer Integrals (all in eV) [Delocalization Parameter $2J/E_{op}$]

polyanions	E_{th}, eV	E_{op}, eV	J, eV	$2J/E_{op}$
$(W_6O_{19})^{3-}$	0.055	1.27	0.38	0.59
$(W_5NbO_{19})^{4-}$	0.075	1.36	0.33	0.48
$(H_2W_{12}O_{40})^{7-}$	0.035	1.04	0.33	0.64
$(SiW_{12}O_{40})^{5-}$	0.035	1.0	0.31	0.62
$(As_2W_{18}O_{62})^{7-}$	0.040	1.38	0.45	0.65
$(AsH_2W_{18}O_{60})^{8-}$	0.040	1.18	0.38	0.64

All tungsten sites are equivalent in the $(W_6O_{19})^{3-}$ and $(XW_{12}O_{40})^{n-}$ structures. This is not, however, the case for $[As_2W_{18}O_{62}]^{7-}$ and $[AsH_2W_{18}O_{60}]^{8-}$ where two kinds of WO_6 octahedra can be distinguished: those belonging to the W_3O_{13} caps and those belonging to the equatorial rings (Figure 1). Several experimental results suggest that the unpaired electron should be trapped on the equatorial tungstens. For instance, the substituted compounds $[P_2W_{17}V^VO_{62}]^{7-}$ and $[P_2W_{17}Mo^{VI}O_{62}]^{6-}$ are more easily reduced when V^V of Mo^{VI} are in equatorial rings (α_1 isomer)[17,18] rather than in the W_3O_{13} caps (α_2 isomer). This localization is also suggested by ^{17}O NMR results on the reduced species[19] $[P_2Mo_{16}Mo_2^VO_{62}]^{8-}$.

Our ESR experiments agree with these results. The g values found for these polyanions are quite different from those found for hexatungstates or dodecatungstates, a result already pointed out by Pope et al.[20] This also suggests a trapping of the unpaired electron on the equatorial tungstens which are specific of the 2/18 structures.

Thermally Activated Electron Hopping. One-electron reduced tungsten polyanions are mixed-valence compounds. A hopping of the unpaired electron between W(V) and W(VI) ions is thus expected. Such a hopping can be thermally activated through the vibrations of the polyanions.[21] The thermal activation energy, however, is quite difficult to measure. In a previous paper, we showed that it could be deduced from a careful analysis of the temperature dependence of the ESR line width.[2] The peak-to-peak line width ΔH_{pp} can be expressed as $\Delta H_{pp(T)} = \Delta H_{pp(0)} + \delta H_{pp(T)}$.

$\Delta H_{pp(0)}$ is the temperature-independent part of the line width. It arises from non-resolved hyperfine interactions, together with dipolar coupling or ligand field distributions. It corresponds to the ESR line width at 0 K and can be deduced from an extrapolation of the $\Delta H_{pp(T)} = f(T)$ curve (Figures 3, 6, and 8).

$\delta H_{pp(T)}$ is the temperature-dependent part of the line width. At high enough temperatures, when the ESR line shape becomes purely Lorentzian, it is governed by a lifetime broadening arising from spin–lattice relaxations induced by the electron hopping.[22] We can then write $\delta H_{pp(T)} = C\nu_h$, where ν_h is the hopping frequency of the unpaired electron and C is a proportionality factor. According to Mott,[23] ν_h follows an exponential law:

$$\nu_h = \nu_0 \exp(-E_{th}/kT)$$

A linear plot of log (δH_{pp}) vs. T^{-1} is actually observed in the high-temperature region (Figure 12). Its slope gives the thermal activation energy of the hopping process. A curvature of this plot is observed at lower temperatures. We did not try to analyze this part of the curve where other relaxation mechanisms could become predominant. The measured activation energies are reported in Table IV.

(16) Kon, H.; Sharpless, N. E. *J. Phys. Chem.* **1966**, *70*, 105. Van Kemenade, J. T. C. *Recl. Trav. Chim. Pays-Bas* **1973**, *92*, 1102.
(17) Acerete, R.; Harmalker, S.; Hammer, C. F.; Pope, M. T.; Baker, L. C. W. *J. Chem. Soc., Chem. Commun.* **1979**, 777.
(18) Contant, R.; Ciabrini, J. P. *J. Inorg. Nucl. Chem.* **1981**, *43*, 1525.
(19) Kazansky, L. P.; Fedotov, M. A. *J. Chem. Soc., Chem. Commun.* **1980**, 644.
(20) Varga, G. M.; Papaconstantinou, E.; Pope, M. T. *Inorg. Chem.* **1970**, *9*, 662.
(21) Hush, N. S. "Mixed Valence Compounds"; Brown, D. B., Ed.; D. Reidel: Dordrecht, 1980; p 151.
(22) Movaghar, B.; Schweitzer, L. *Phys. Status Solidi B* **1977**, *80*, 421.
(23) Austin, I. G.; Mott, N. F. *Adv. Phys.* **1969**, *18*, 41.

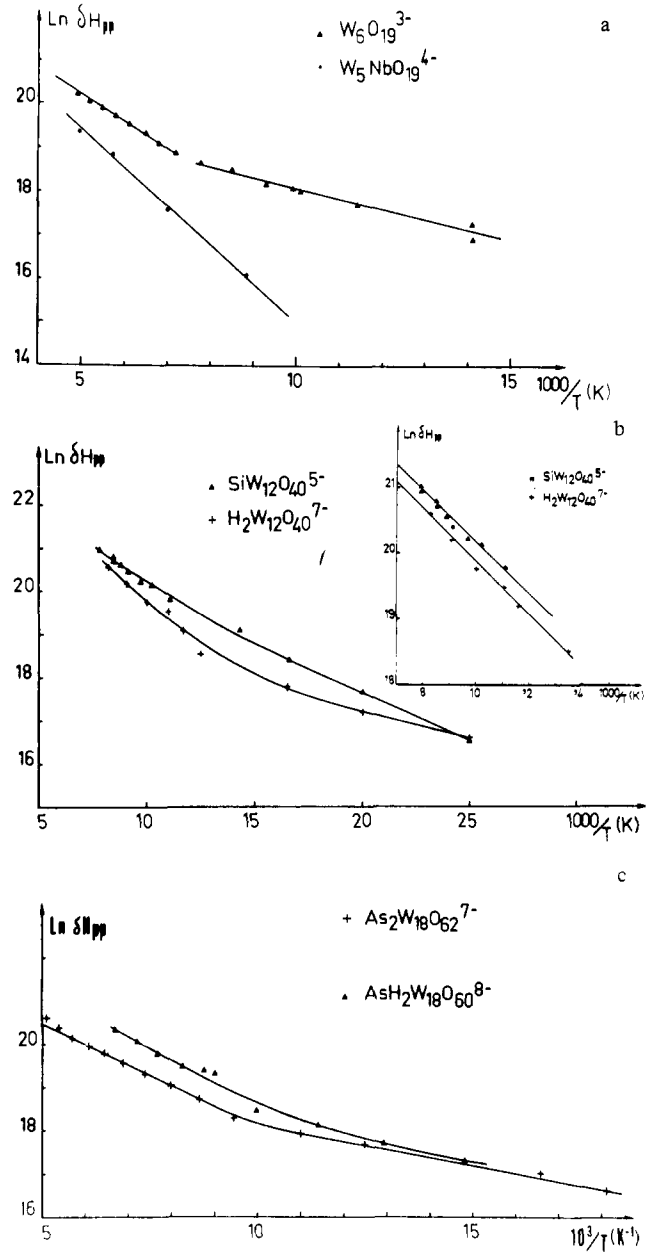

Figure 12. Plot of ln $\delta H_{pp} = f(T^{-1})$ where δH_{pp} corresponds to the temperature-dependent part of the ESR line width: (a) (▲) $(W_6O_{19})^{3-}$, (●) $(W_5NbO_{19})^{4-}$; (b) (+) $(H_2W_{12}O_{40})^{7-}$, (▲) $(SiW_{12}O_{40})^{5-}$; (c) (+) $(As_2W_{18}O_{62})^{7-}$, (▲) $(AsH_2W_{18}O_{60})^{8-}$.

These results show that electron delocalization appears to be more difficult (the thermal activation energy increases) in the M_6O_{19} structures. The observed differences between dodecatungstates and octadecatungstates do not appear to be significant.

Electronic Spectra. $[W_6O_{19}]^{3-}$ and $[NbW_5O_{19}]^{4-}$. The observed band positions fall into the usual range for the d–d transitions $^2B_2 \rightarrow {}^2E$ and $^2B_2 \rightarrow {}^2B_1$ in C_{4v} symmetry. Therefore, no unambiguous identification of an intervalence band is possible. In the related molybdenum species $[Mo_6O_{19}]^{3-}$, we have assigned a shoulder at 9000 cm^{-1} to an intervalence band.[2,10] It is thus likely that in the present systems, the intervalence band and the d–d $^2B_2 \rightarrow {}^2E$ transition overlap and account for the 10 000-cm^{-1} band. The second d–d transition ($^2B_2 \rightarrow {}^2B_1$) would correspond to the peak near 25 000 cm^{-1}. The shoulder at 19 000 cm^{-1} in $[W_6O_{19}]^{3-}$ remains unexplained. It is tempting to attribute it to the same impurity observed by ESR (see above). However, this spectrum has been found identically in different media (dimethylformamide, acetonitrile, dimethyl sulfoxide, and a dimethylacetamide/methanol mixture). Finally, the spacing between the shoulders observed on the edge of the 10 000-cm^{-1} band of $[W_6O_{19}]^{3-}$ (1100, 1200, and 1400 cm^{-1}) seems too high to be attributed to a vibrational progression. They could perhaps be explained by a splitting of the intervalence band due to the high number of tungsten atoms in the structure[24] (exciton structure).

$[SiW_{12}O_{40}]^{5-}$ and $[H_2W_{12}O_{40}]^{7-}$. For these compounds, the band at 8000 cm^{-1} falls outside the usual range for d–d transitions and thus can safely be assigned to an intervalence transition. The other bands are probably due to the d–d transitions with increased intensities, but could also contain intervalence components (see the discussion for molybdates[2]).

$[As_2W_{18}O_{62}]^{7-}$ and $[AsH_2W_{18}O_{60}]^{8-}$. The lowest energy band (near 5700 cm^{-1}) and probably also the second one (near 10 000 cm^{-1}) are assigned to intervalence transitions. The particularly low energy of the first band seems to be related to the structural pecularities of the octadecatungstate species, which present corner sharing pairs of WO_6 octahedra with almost linear W–O–W bridges. This type of junction links the two halves of the molecule (see Figure 1). Supporting this conclusion we recently observed low-energy intervalence bands in the $[W_{10}O_{32}]^{5-}$ polyanion for which similar junctions have been reported. The origin of these low-energy intervalence bands will be discussed below.

Electronic Interactions. According to eq 1 the transfer integral J between adjacent metallic sites can be deduced from a comparison of the thermal and optical activation energies:

$$J = \tfrac{1}{2}E_{op} - (E_{th} \times E_{op})^{1/2}$$

The results of such a determination are gathered in Table IV. These values have to be analyzed carefully. They can only given an approximate value because the optical activation energy is only deduced from the position of the maximum of the intervalence band. A detailed analysis of this absorption band is necessary in order to obtain reliable results.

However, they show that electron delocalization is more difficult in the M_6O_{19} structure. This, together with the well-resolved hyperfine structure seen on ESR spectra and the weak intensity of the optical bands, agrees with previous results on molybdenum polyanions.[2] Delocalization appears easier in the $(XW_{12}O_{40})$ structure. We have shown elsewhere[2] that this could be attributed to the corner sharing mode of junction linking different W_3O_{13} groups. An easier delocalization through corner sharing octahedra can also be deduced from low-temperature ESR experiments. We have shown that g_x and g_y first collapse leading to an axial spectrum. This shows that the x and y directions are first averaged while the z axis remains almost unchanged. Such a result could be explained if we assume that the unpaired electron is first delocalized between corner sharing octahedra belonging to three different W_3O_{13} groups.

An even stronger delocalization is likely to occur in both octadecatungstates, for the following reasons: (i) the intensity of electronic bands is very high, (ii) the equatorial sites which are reduced first are linked across the two halves of the molecule by almost linear W–O–W bridges which should lead to an efficient orbital overlap, and (iii) these equatorial sites do not form triangular moieties as in the Keggin structure. Indeed it has been shown theoretically that the occurrence of a triangular group of metal atoms linked by O^{2-} ions prevents a complete delocalization over the whole group.[25] For the type of junctions encountered in heteropolyanions, the delocalization should be easier when only binuclear groups are present, which is the case in the equatorial region of the octadecatungstates. We thus consider the possibility of a complete delocalization on two[26] adjacent tungsten atoms

(24) Hush, N. S. *Prog. Inorg. Chem.* **1967**, *8*, 391.
(25) Launay, J. P.; Babonneau, F. *Chem. Phys.* **1982**, *67*, 295.
(26) A complete delocalization on four tungsten atoms (as in $[W_4O_8Cl_8(H_2O)_4]^{2-}$) is considered unlikely for the following reason: In the $[As_2W_{18}O_{62}]^{7-}$ structure, it is effectively possible to find an approximately square array of four tungsten atoms linked by corner sharing only, since the two halves of the molecule are related by a mirror plane. However, this is not possible with the $[AsH_2W_{18}O_{60}]^{8-}$ structure in which the two halves are related by an inversion center.
(27) Cannon, R. D., ref 3b, p 186.
(28) Sanchez, C.; Livage, J.; Doppelt, P.; Chauveau, F.; Lefebvre, J. *J. Chem. Soc., Dalton Trans.* **1982**, *9*, 835.

belonging to the two halves of the molecule. This would be consistent with the absence of hyperfine structure and would explain the orthorhombic ESR spectra as well. Moreover, this hypothesis would also explain the occurrence of low-energy intervalence bands near 6000 cm^{-1} which is otherwise difficult to rationalize. They could correspond to an electron transfer between *two such pairs* of tungsten atoms. In the Appendix, we show that this process should occur at an energy about half the usual value for intervalence bands. Physically, this results from the spreading of the distortion associated with the electron over two sites, decreasing the effective electron–phonon coupling constant. The other band, near 10000 cm^{-1}, would then be the intervalence transition between delocalized levels inside the W–W pair. This would give a J parameter of $10000/2 = 5000$ cm^{-1}. Such a model of course remains purely speculative as long as no experimental results give any proof of such a delocalization in a W–W pair.

Substitution in the W_6O_{19} Structure. It might be interesting to analyze in some detail the effect of a substitution in the W_6O_{19} structure where all tungsten sites are equivalent. This was done with $(NbW_5O_{19})^{4-}$ where one W(VI) was replaced by a Nb(V) ion. As a result of this we now have two different kinds of tungsten sites: four of them are situated in the ring sharing edges with the NbO_6 octahedra and one is on the opposite side sharing only one corner.[15]

This would introduce a new energy term W corresponding to the non-symmetric case in the P.K.S. model.[3] As shown by these authors this could lead to an increase of the energy of the intervalence band in the optical spectrum. A 600-cm^{-1} shift toward higher energy is actually observed. The thermal activation energy should also increase and this is actually suggested by a comparison of both ESR experiments.

$$E_{th} = 0.05 \text{ eV for } [W_6O_{19}]^{3-}$$

$$E_{th} = 0.07 \text{ eV for } [NbW_5O_{19}]^{4-}$$

Low-temperature ESR spectra show that in both $[W_6O_{19}]^{3-}$ and $[NbW_5O_{19}]^{4-}$ the unpaired electron remains localized on a single tungsten site. The ligand field symmetry around this tungsten atom appears axial in the first case and othorhombic in the second one. This could be due to a modification of the symmetry of the whole polyanion. The very large line width observed in the case of $[NbW_5O_{19}]^{4-}$ could be attributed to a non-resolved super-hyperfine coupling with the Nb nucleus ($I = {}^9/_2$).

Acknowledgment. The technical assistance of D. Simons is gratefully acknowledged.

Appendix I

Let us consider the binuclear system AB below and assume that M_A is in the oxidation state VI and M_B is in the oxidation state V. The bond distances are initially r_{VI} around M_A and r_V around

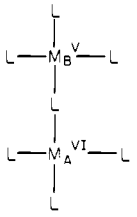

M_B. The optical excitation yields of M_A^V ion in an environment of M^{VI} and vice versa, so that we can write

$$E_{opt} = \frac{n}{2}k_V(r_V - r_{VI})^2 + \frac{n}{2}k_{VI}(r_V - r_{VI})^2 \qquad (2)$$

where n is the number of bonds around a given ion and k_V and k_{VI} are the metal ligand force constants. E_{op} thus depends only on force constants and the bond length variation upon a change in oxidation state. It does not depend upon the electron-transfer integral, as long as the system remains localized (class II).[3] Usually, the force constants are not very different, so that (2) can be written:

$$E_{op} = nk(r_V - r_{VI})^2 = nk\Delta r^2 \qquad (3)$$

If now we assume that the A–B system is completely delocalized in the ground state (as a result of a strong electronic interaction between M_A and M_B), the bond lengths will all have the same "average value" given by:[27]

$$r^* = \frac{r_{VI}k_{VI} + r_Vk_V}{k_{VI} + k_V}$$

which, taking into account our hypothesis on force constants, simplifies to

$$r^* = (r_{VI} + r_V)/2 \qquad (4)$$

An intervalence transition can now occur between two such AB units, according to

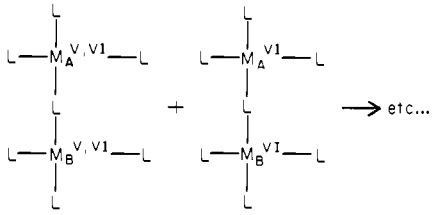

This is equivalent to an intervalence transition between mononuclear units, with effective $\Delta r'$ and n' given by

$$\Delta r' = r^* - r^{VI} = \Delta r/2$$

$n' =$
$2n$ (since there are twice as many bonds to be rearranged)

Then eq 3 leads to

$$E_{op}' = E_{op}/2$$

i.e., the energy of the intervalence transition between delocalized binuclear units is half the energy of the usual process between mononuclear units.

Registry No. $(W_6O_{19})^{3-}$, 62185-91-5; $(W_2NbO_{19})^{4-}$, 62185-89-1; $(H_2W_{12}O_{40})^{7-}$, 12501-12-1; $(SiW_{12}O_{40})^{5-}$, 12504-06-2; $(As_2W_{18}O_{62})^{7-}$, 59965-04-7; $(AsH_2W_{18}O_{60})^{8-}$, 87226-36-6.